

4-[3-(4-Cyclopropanecarbonylpiperazine-1-carbonyl)-4-fluorobenzyl]-2H-phthalazin-1-one: A Novel Bioavailable Inhibitor of Poly(ADP-ribose) Polymerase-1

Keith A. Menear,^{*,†} Claire Adcock,[†] Robert Boulter,[†] Xiao-ling Cockcroft,[†] Louise Copsey,[†] Aaron Cranston,[†] Krystyna J. Dillon,[†] Jan Drzewiecki,[†] Sheila Garman,[†] Sylvie Gomez,[†] Hashim Javid,[†] Frank Kerrigan,[‡] Charlotte Knights,[†] Alan Lau,[†] Vincent M. Loh, Jr.,[†] Ian T. W. Matthews,[†] Stephen Moore,[†] Mark J. O'Connor,[†] Graeme C. M. Smith,[†] and Niall M. B. Martin^{*,†}

KuDOS Pharmaceuticals Ltd., 410 Cambridge Science Park, Milton Road, Cambridge, U.K. CB4 0PE, and Thermo Fisher Scientific Ltd., Trevillet, Tintagel, Cornwall, U.K. PL34 0HW

Received February 6, 2008

Poly(ADP-ribose) polymerase activation is an immediate cellular response to metabolic-, chemical-, or ionizing radiation-induced DNA damage and represents a new target for cancer therapy. In this article, we disclose a novel series of substituted 4-benzyl-2H-phthalazin-1-ones that possess high inhibitory enzyme and cellular potency for both PARP-1 and PARP-2. Optimized compounds from the series also demonstrate good pharmacokinetic profiles, oral bioavailability, and activity in vivo in an SW620 colorectal cancer xenograft model. 4-[3-(4-Cyclopropanecarbonylpiperazine-1-carbonyl)-4-fluorobenzyl]-2H-phthalazin-1-one (KU-0059436, AZD2281) **47** is a single digit nanomolar inhibitor of both PARP-1 and PARP-2 that shows standalone activity against BRCA1-deficient breast cancer cell lines. Compound **47** is currently undergoing clinical development for the treatment of BRCA1- and BRCA2-defective cancers.

Introduction

Poly(ADP-ribose) polymerase-1, or PARP-1^a, is a 113 kDa nuclear protein that is involved in the signaling of DNA damage through its ability to recognize and rapidly bind DNA single- or double-strand breaks.¹ PARP-1 is also known to participate in a variety of cellular functions, including gene amplification and transcriptional regulation, cell division, and differentiation as well as apoptosis and chromosome stability.^{2,3} PARP-1 is the most abundant protein of a family of some 18 proteins that are now identified.^{4,5} Its closest homolog is PARP-2, which is ~62% identical in its catalytic domain to PARP-1, and unlike the rest of the PARP family, it also has the ability to bind DNA and compensate for PARP-1 activity in DNA single-strand break (SSB) repair.⁶ Other PARP superfamily members include vault PARP, which participates in macroparticle excretion through its inclusion in vault bodies, and the more extensively studied polyribosylating protein tankyrase (of which there are two distinct proteins), which helps regulate telomerase activity at the chromosomal telomere tails.^{7,8}

Studies on the mechanism by which PARP-1 modulates DNA repair and other processes have identified its ability to produce long chains of poly(ADP-ribose) (PAR) within the cell nucleus as being central to its activity.⁹ Following DNA damage, PARP-1 is rapidly activated by binding to DNA breaks, where

it utilizes NAD⁺ to synthesize poly(ADP)ribose chains either on itself (poly(ADP)ribosylation) or on a variety of nuclear target proteins, including topoisomerases, histones, and p53.^{1,10} This process of PARP-1 binding and activation helps amplify the repair process that is known as base excision repair (BER) in which SSBs are targeted. SSBs are generally introduced into the DNA by oxidative damage that are caused by the cell's own metabolic processes as well as by exogenous chemical damage or ionizing radiation. PARP-1 knockout (PARP ^{-/-}) cells and animals exhibit high sensitivity when they are exposed to alkylating agents and γ irradiation.^{11,12} Moreover, in studies that use low-molecular-weight inhibitors of PARP-1, it has been shown that the effects of radiation are enhanced by the suppression of the repair of potentially lethal DNA damage.^{13,14} In cells that are treated with alkylating agents, the inhibition of PARP-1 leads to a marked increase in DNA strand breakage and cell killing.^{15,16} The use of more recent selective and potent PARP-1 inhibitors has confirmed that the inhibition of PARP-1 activity potentiates a wide variety of important cancer cytotoxins including 3,4-dihydro-3-methyl-4-oxoimidazo[5,1-*d*]-as-tetrazine-8-carboxamide (temozolomide (TMZ)), tecans such as (S)-10-[(dimethylamino)methyl]-4-ethyl-4,9-dihydroxy-1H-pyrano[3,4:6,7]indolizino[1,2-*b*]quinoline-3,14-(4*H*,12*H*)-dione (topotecan), and *cis*-diamminedichloroplatinum(II) (cisplatin).^{17–21}

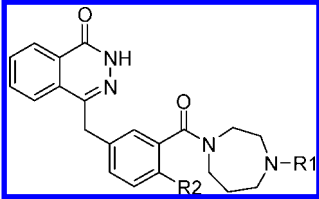
The potential of PARP inhibition within oncology was further highlighted by reports that cell lines deficient in BRCA1 and BRCA2 (proteins involved in homologous recombination (HR) repair²²) are highly sensitive to PARP-1 inhibitors resulting in cell death.^{23,24} BRCA1 and BRCA2 are known tumor suppressor genes whose wild-type alleles are frequently lost in tumors of heterozygous carriers.^{25,26} The association of BRCA1 and BRCA2 protein mutations with breast cancer is well characterized.²⁷ Carriers of mutations in BRCA1 and BRCA2 are also at an elevated risk of cancer of the ovary, prostate, and pancreas. Therefore, the possibility exists that PARP-1 inhibitors will be of high therapeutic benefit for tumors that are deficient in these specific proteins and potentially for other DNA-repair HR proteins that may be lost within the tumorigenesis process.^{28–30}

* To whom correspondence should be addressed. (K.A.M.) E-mail: kmenear@kudospharma.co.uk. (N.M.B.M.) Tel: (44) 1223 719 719. Fax: (44) 1223 719 720. E-mail: nmartin@kudospharma.co.uk.

[†] KuDOS Pharmaceuticals Ltd.

[‡] Thermo Fisher Scientific Ltd.

^a Abbreviations: PARP, poly(ADP-ribose)polymerase; SSB, single-strand break; BER, base excision repair; DSB, double-strand break; HR, homologous recombination; MMS, methyl methanesulfonate; PAR, poly(ADP-ribose); TMZ, temozolomide; RTV, relative tumor volumes; Boc, *tert*-butoxycarbonyl; DMSO, dimethylsulfoxide; TFA, trifluoroacetic acid; DCM, dichloromethane; DMA, dimethyl acetamide; DMF, dimethyl formamide; ether, diethyl ether; Et₃N, triethylamine; EtOH, ethanol; HCl, hydrochloric acid; h, hours; IPA, isopropyl alcohol; THF, tetrahydrofuran; DIPEA, *N,N'*-diisopropylethylamine; NH₄OH, ammonium hydroxide; MeOH, methanol; NaOH, sodium hydroxide; HBTU, 2-(1*H*-benzotriazole-1-yl)-1,1,3,3-tetramethyluronium hexafluorophosphate.

Table 1. PARP-1 and Cellular Potencies of the Homopiperazine Series


compd	R1	R2	PARP-1 IC ₅₀ (μM)	PF ₅₀ ^a
14	H	F	0.007	12.6
15	2-hydroxyethyl	H	0.018	5.4
16	2-hydroxyethyl	F	0.007	18.0
17	benzyl	H	0.018	2.2
18	ethylsulfonyl	H	0.023	1.4
19	morpholine-4-carbonyl	H	0.020	1.4
20	morpholine-4-carbonyl	F	0.008	2.5
21	acetyl	F	0.012	3.7
22	cyclopropanecarbonyl	F	0.012	4.2

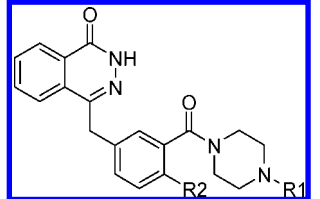
^a The PF₅₀ value is the potentiation factor and is calculated as the ratio of the IC₅₀ growth curve for the alkylating agent methyl methanesulphonate (MMS) divided by the IC₅₀ of the curve of MMS + PARP inhibitor (Experimental Section). The cells used were HeLaB, and the test compounds were used at a fixed concentration of 200 nM. PARP-1 IC₅₀ and PF₅₀ values are means from two to three independent dose-response curves. Variation was generally ±1% for PARP-1 and ±15% for PF₅₀.

PARP activity was initially described over 40 years ago, and since then there has been significant activity in the search for pharmaceutically relevant inhibitors.^{3,31} However the correct selection of inhibitor and clinical context has proven to be difficult. To date, there are no drugs that modulate the target that have reached the market, although a number of preclinical and clinical agents are now being actively pursued, particularly in cancer in combination therapy with established DNA-damaging agents.³¹ These include Pfizer and the University of Newcastle's 8-fluoro-2-(4-methylaminomethylphenyl)-1,3,4,5-tetrahydroazepino[5,4,3-*cd*]indol-6-one (AG014699)³² and Inotek Pharmaceuticals' undisclosed INO-1001,³³ both for intravenous administration, and Abbott's orally available 2-[(*R*)-2-methylpyrrolidin-2-yl]-1*H*-benzimidazole-4-carboxamide (ABT-888).³⁴

4-[3-(4-Cyclopropanecarbonylpiperazine-1-carbonyl)-4-fluorobenzyl]-2*H*-phthalazin-1-one (**47**) is a novel, potent, and orally bioavailable inhibitor of PARP-1 that has demonstrated exciting clinical efficacy as a monotherapy in *BRCA1*- and *BRCA2*-deficient ovarian and breast cancers.³⁵ It is also under clinical investigation in combination with DNA-damaging agents including 5-(3,3-dimethyl-1-triazenyl)-1*H*-imidazole-4-carboxamide (dacarbazine) and *cis*-diamine(1,1-cyclobutanedicarboxylato)platinum(II) (carboplatin). The following discussion describes the potency refinement and the pharmacokinetic (PK) optimization of a series of 4-benzyl-2*H*-phthalazin-1-ones leading to the identification of **47**.

Chemistry

The synthesis of both the piperazine and the homopiperazine analogs that are described in Tables 1–4 was achieved via amide bond coupling of the corresponding 3-[(4-oxo-3*H*-phthalazin-1-yl)methyl]benzoic acid **7** or 2-fluoro-5-[(4-oxo-3*H*-phthalazin-1-yl)methyl]benzoic acid **8** (Scheme 1). The synthesis of corresponding intermediate **7** is outlined in Scheme 1. The nucleophilic addition of 3*H*-isobenzofuran-1-one **1** to 3-formylbenzonitrile **2** in the presence of sodium methoxide provided 3-(1,3-dioxindol-2-yl)benzonitrile **3** in good yield. The reaction of indanone **3** with hydrazine hydrate provided the primary phthalazinone core that, after base hydrolysis, furnished the key

Table 2. PARP-1 and Cellular Potencies of Piperazine Series **23–38**


compd	R1	R2	PARP-1 IC ₅₀ (μM)	PF ₅₀
23	H	H	0.002	3.7
24	H	F	0.005	8.6
25	2-pyridyl	H	0.010	24.3
26	2-pyridyl	F	0.002	>40 ^a
27	2-pyrimidinyl	H	0.002	>40 ^a
28	2-pyrimidinyl	F	0.003	>40 ^a
29	ethylsulfonyl	H	0.012	4.6
30	ethylsulfonyl	F	0.008	4.9
31	morpholine-4-carbonyl	H	0.008	2.3
32	morpholine-4-carbonyl	F	0.006	8.4
33	phenyl	H	0.051	ND
34	phenyl	F	0.005	5.2
35	benzoyl	H	0.011	7.2
36	benzoyl	F	0.006	8.2
37	2-hydroxyethyl	H	0.039	1.8
38	2-hydroxyethyl	F	0.012	3.3

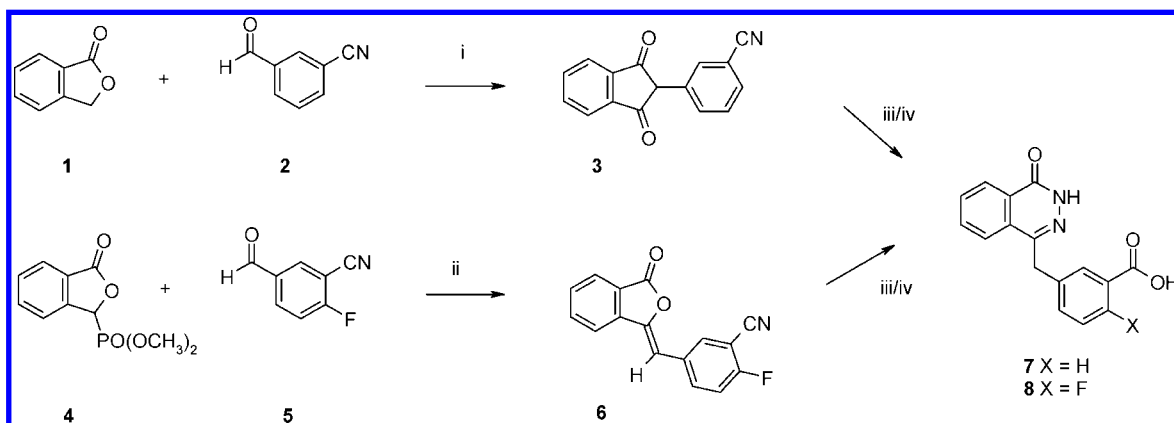
^a A PF₅₀ value of >40 is indicative of a compound that causes complete sensitization to MMS at a fixed concentration of 200 nM.

acid intermediate **7**. For the corresponding fluoro analog **8**, in which the fluoro that is ortho to the nitrile group is labile to nucleophilic displacement, an alternative milder methodology starting from 3-dimethoxyphosphoryl-3*H*-2-benzofuran-1-one **4** was required. As such, the commercially available phosphonate **4** was coupled to 2-fluoro-5-formylbenzonitrile **5** under standard conditions to produce 2-fluoro-5(3-oxo-3*H*-isobenzofuran-1-ylidenemethyl)benzonitrile **6**. A mixture of *E* and *Z* isomers are isolated without separation and were treated with hydrazine hydrate to produce the phthalazinone core. Base hydrolysis of the pendant nitrile provides the second key carboxylic acid intermediate **8**.

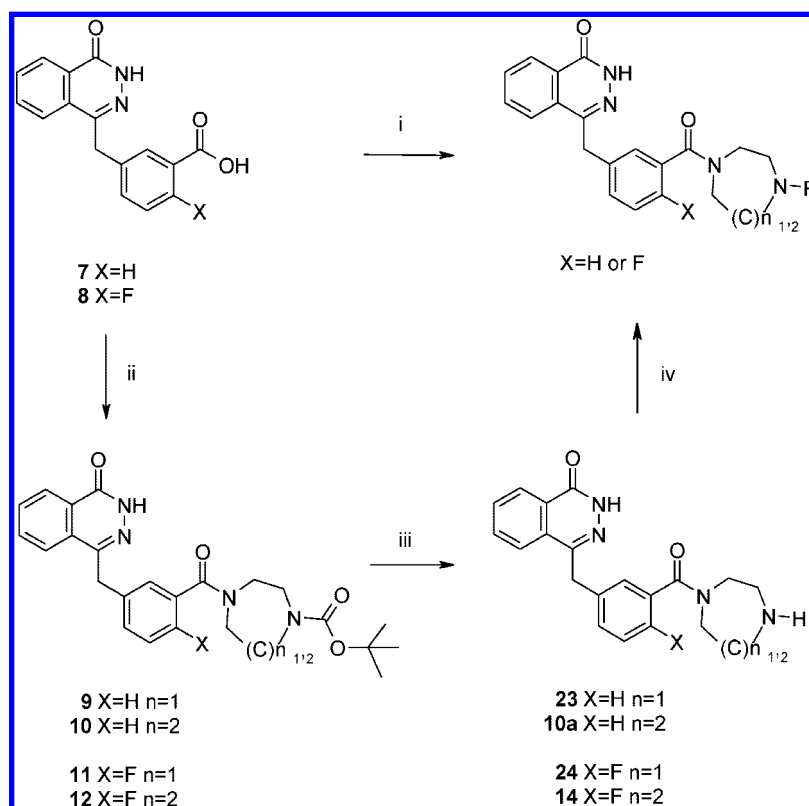
With the fluoro and des-fluoro carboxylic phthalazinones in hand, we established the chemistry to enable small focused libraries to be generated by one of two methods (Scheme 2). For a number of the piperazine and homopiperazine analogs, the appropriately functionalized amine was coupled to the acid with HBTU to provide reliably high yields of the target amides. Alternatively, fluoro or des-fluoro carboxylic phthalazinones **7** or **8** were reacted with either Boc-piperazine or Boc-homopiperazine to produce amides **9–12**. Deprotection under acid conditions yielded either the piperazine or homopiperazine-carbonyl-benzylphthalazinone **10a**, **14**, **23**, or **24**, which were suitable for further elaboration by parallel synthesis. As such, standard conditions were employed in providing the alkyl, acyl, aryl, sulfonamide, and urea derivatives that are described in Tables 1–4.

Results and Discussion

Previously, we and others have described the identification, synthesis, and optimization of a number of potent inhibitors of PARP-1 that bear a common phthalazinone core.^{36–40} The focus of these efforts was to optimize hits, which originated from a medium throughput screen, that identified benzyl phthalazinone **13** as a moderately potent (IC₅₀ = 0.77 μM) PARP-1 antagonist (Figure 1). A liability of the early compounds in the series was a lack of cellular activity, which was measured by their ability to sensitize HeLa B cells to the killing effect of the alkylating

Scheme 1. Synthesis Route for Phthalazinone Acid Intermediates **7** and **8**^a

^a (i) Ethyl propionate, NaOMe, MeOH, reflux; (ii) Et₃N, THF, RT; (iii) (a) NaOH(aq), THF, 72 h, 100 °C and (b) HCl (2 N); and (iv) NH₂NH₂·H₂O, 3 h, reflux.

Scheme 2. Synthesis Route for Phthalazinone Piperazine and Homopiperazine Analogs^a

^a (i) HBTU, substituted (homo)piperazine, DIPEA, DCM; (ii) HBTU, *tert*-butyl (homo)piperazine-1-carboxylate, DIPEA, DMA; (iii) 6 N HCl, EtOH; and (iv) ROCl or RSO₂Cl or RNCO, DIPEA, DCM or RCO₂H, HBTU, DIPEA or NaBH₄, RCHO.

agent methyl methanesulfonate (MMS). This issue was resolved by the optimization of the pendant benzyl linker to provide potent inhibitors of PARP-1 at both the enzyme and the cellular level. In addition, the intrinsic pharmacokinetics of the series were improved to yield good in vitro and in vivo half lives, which culminated in the disclosure of 4-[[3-(1,4-diazepane-1-carbonyl)-4-fluorophenyl]methyl]-2*H*-phthalazin-1-one **14**.

The focus of our efforts that lead to the identification of homopiperazine **14** was to provide a clinically useful PARP-1 inhibitor for use in combination with known cytotoxic agents following iv administration. However, we reasoned that clinical utility and patient compliance would be significantly enhanced by the development of an orally available inhibitor of PARP-1 that would be suitable for longer-term treatments as a mono-

therapy or in combination. As the subject of this article, our efforts were concentrated on the introduction of oral bioavailability to the benzylphthalazinone series.

To reach this objective, we established the chemistry to afford ready access to a number of designed focused libraries. Not all data are represented here, and only compounds that are illustrative of the key structure–activity relationships (SARs) are discussed. From the activities described below, over 1000 compounds were generated, 87 and 43% of which had PARP-1 IC₅₀ values that were <50 and <10 nM, respectively, and 53% that had a PF₅₀ value of >2. Throughout the library design process, consideration was given to the key physicochemical properties that might influence oral absorption. In particular, we made efforts to limit the molecular weight and the polar

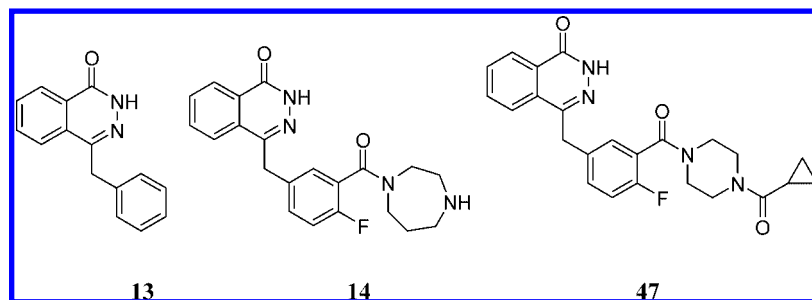


Figure 1. Structures of 4-benzyl-2*H*-phthalazin-1-one **13**, homopiperazine analog **14**, and clinical candidate **47**.

surface area (<550 and <140 Å², respectively) together with the number of rotatable bonds (<7), the total number of hydrogen-bond donors/acceptors (<10), the lipophilicity, and the pK_a (basic <8) while continuing to maintain the necessary solubility (>0.1 mg/mL).⁴¹

We reasoned that a key impediment to oral availability in **14** was the high pK_a (calculated value of 9.87) of the distal nitrogen on the homopiperazine side chain. Previous investigators have designed inhibitors of PARP-1 to mimic the substrate–protein interactions of NAD⁺ with the enzyme.¹⁷ Mechanistically, these compounds inhibit PARP-1 by blocking the binding of the substrate, particularly the nicotinamide moiety, to the active site. Early weak inhibitors such as 3-aminobenzamide⁴² have been developed into more potent PARP-1 inhibitors that are derived from a range of related pharmacophoric templates. Through a previously developed SAR, we reasoned that compound **14** similarly binds into the nicotinamide substrate binding pocket of the active site of PARP-1 and makes a key bidentate interaction with Ser904 and Gly863, which is characteristic of this class of pharmacophore. Additionally, this binding pose suggests that the functionalization of the homopiperazine is well tolerated without detrimental effects on enzyme activity. This makes it possible to modulate the physicochemical properties of compound **14** by the appropriate substitution at the distal nitrogen.

To this effect, 2-hydroxyethyl derivatives **15** and **16** were synthesized to induce a reduction in the pK_a of the basic nitrogen via the β effect of the side-chain oxygen (Table 1). Typically, analogs were made in both the 4-fluoro and des-fluorobenzyl series for comparison. The resulting compounds **15** and **16** illustrate that alkylation at N4 is tolerated with the preservation of good enzyme and cell potency. The N4 benzyl-substituted compound **17** continues to maintain PARP activity, albeit with only modest cellular potency. The removal of the entire basic center with the sulfonamide and urea derivatives **18**, **19**, and **20** demonstrated that the cationic center is not a prerequisite for activity although cellular potency is reduced vis-a-vis compound **14**. Likewise, acyl adducts **21** and **22** maintain good PARP-1 activity but are similarly compromised against cell activity compared to **14**, which is possibly due to limited cellular permeability.

In a logical extension to the homopiperazine series, a number of corresponding piperazine analogs were explored (Table 2). Interestingly, in the direct comparison with homopiperazine **14**, compound **24** is equipotent for PARP-1 but is marginally less active in the cellular sensitization assay ($PF_{50} = 12.6$ vs 8.6, respectively), which may be indicative of a reduction in cell permeability. However, as anticipated, the side-chain SARs are broadly superimposable. Again, the tactic of N4 substitution with piperazine side chains that are designed to modulate permeability/absorption characteristics was employed. The attachment of heterocyclic groups in both the fluoro and des-

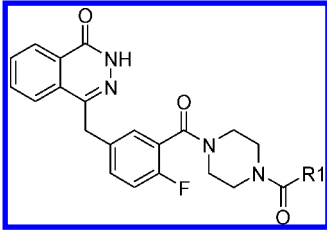
Table 3. PARP-1 and Cellular Potencies of Alkylpiperazines **39–44**

compd	R1	R2	PARP-1 IC ₅₀ (μM)	PF ₅₀
24	H	F	0.005	8.6
39	methyl	H	0.088	1.02
40	methyl	F	0.013	2.5
41	ethyl	F	0.006	7.7
42	<i>n</i> -propyl	F	0.006	7.3
43	<i>n</i> -butyl	F	0.005	6.4
44	cyclopropylmethyl	F	0.004	6.5

fluoro series furnished the 2-pyridyl and 2-pyrimidinyl analogs **25–28**, respectively. Both substitutions gave highly potent PARP-1 inhibitors ($IC_{50} < 5$ nM) with significant improvements in cellular activity over the matched fluoro compound **24** and unsubstituted compound **23**. Ethylsulfonamide **29** was more successful in the piperazine series (cf. homopiperazine sulfonamide **18**), which was also true for urea derivatives **31** and **32**. A loss of enzyme potency is observed when R1 is phenyl and R2 is hydrogen (compound **33**), although this is regained 10-fold when R2 is replaced by fluorine (compound **34**). Benzoyl compounds **35** and **36** show that the enzyme can tolerate reasonably large functionality while maintaining potency although entries **37** and **38**, corresponding to the homopiperazine 2-hydroxyethyl analogs **15** and **16**, show a reduction in absolute PF_{50} values (i.e., $PF_{50} = 18$ and 3.3 for compounds **16** and **38**, respectively).

The influence of the 4-fluorine substitution has been previously noted, but is particularly evident in this series. A matched-pair analysis shows a mean PF_{50} difference of 2.67, which is a significant enhancement over that of the 4-hydrogen. The similar enzyme potencies suggest that the introduction of a fluorine at C-4 on the benzyl linker enhances the permeability. Interestingly, this does not appear to be a global change in molecular properties because the introduction of a fluorine at positions other than the benzyl C-4 (data not shown) does not replicate this effect. A possibility may be that repulsive dipole–dipole interactions with the pendant C-3 carbonyl may restrict conformational rotation and molecular entropy, which leads to a more permeable compound.

Beyond this observation, convincing structure- PF_{50} relationships have been elusive within the phthalazinone series. Modest changes to structure can have unanticipated effects on PF_{50} values, and, despite the analysis of a large data set, correlations of PF_{50} with permeability parameters such as lipophilicity and solubility have been disappointing. A set of piperazine deriva-

Table 4. PARP-1 and Cellular Potencies of Acylpiperazines **45–51**


compd	R1	PARP-1 IC ₅₀ (μM)	PF ₅₀
45	methyl	0.006	7.97
46	ethyl	0.005	24.4
47	cyclopropyl	0.005	25.8
48	cyclopentyl	0.002	11.8
49	cyclohexyl	0.015	11.1
50	2-tetrahydrofuryl	0.003	39.4
51	3-tetrahydrofuryl	0.002	29.8

Table 5. IC₅₀ Measurements of Compound **47** against PARP-1, PARP-2, and Tankyrase-1

enzyme	IC ₅₀ (μM) ^a
PARP-1	0.005
PARP-2	0.001
tankyrase-1	1.5

^a Values are means from two to three independent dose-response curves. Variation was generally ±1% for PARP-1 and -2 and ±15% for tankyrase-1.

tives that did show transferable PF₅₀ profiles is illustrated in Table 3. Here simple alkyl homologation provides compounds with a significant increase in cellular activity from C-1 to C-2 elongation (compounds **39–41**). The SAR for the series shows an optimum cellular activity that decreases as lipophilicity increases (compounds **42–44**), and within this compound set, only ethyl **41** (PF₅₀ = 7.7) approaches the activity of simple unsubstituted compound **24**. The pattern of activity that is represented by **39** to **41** in Table 3 was transferable to an alternative amide series that is outlined in Table 4. Acylation of **24** to produce 4-acetyl piperazine **45** provided a compound with good enzyme and cell-kill enhancement. As previously described for the alkyl-capped piperazines (Table 3), the fine-tuning of the R1 aliphatic side chain to ethyl **46**, cyclopropyl **47**, cyclopentyl **48**, and cyclohexyl **49** gave excellent enhancement in PF₅₀ over acetyl alone. Furthermore, the introduction of a 2- or 3-tetrahydrofurylamide group (**50** and **51**, respectively) enhances both PF₅₀ and aqueous solubility (0.98 mg/mL for **50**). It is interesting that there is a significant enhancement in both enzyme and cell potency for cyclopropylamide **47** in comparison with that for its homopiperazine counterpart **22** (IC₅₀ = 12 vs 5 nM and PF₅₀ = 4.2 vs 25.8, respectively).

The selectivity profile of **47** is typical of the inhibitors tested in this class (Table 5). As expected from the close homology between PARP-1 and PARP-2, **47** is essentially equipotent against the two PARP isoforms, whereas it is 300 times less effective against the inhibition of tankyrase.

As had been alluded to earlier, the discrimination of compounds on the basis of potency or selectivity alone was problematic because of the high number of actives that were generated. Therefore, in an effort to address the objective of finding an orally bioavailable PARP-1 inhibitor, we utilized a medium-throughput mouse in vivo pharmacokinetic assay. Typically, inhibitors were administered both iv (data not shown) and po. Samples were collected over only limited time points, and inhibitor plasma levels at 30 and 60 min were predominantly used for ranking. Representative data are provided in Table 6,

Table 6. Pharmacokinetic Screen of Representative Compounds in Mouse^a

compd	plasma concn (μg/mL)	
	30 min	60 min
27	0.30	0.14
34	0.70	0.31
46	0.67	0.30
47	0.23	0.59
50	0.28	0.13
51	0.16	0.15

^a Compound dosed po at 10 mg/kg in vehicle 10% DMSO/10% cyclodextrin in PBS.

Table 7. Pharmacokinetics of Compound **46** in Rat and Compound **47** in Rat and Dog

compd	46	47	
	rat ^a	rat ^a	dog ^b
T _{1/2} (min)	55	53	170
Cl (mL/min/kg)	35.4	49	5.4
AUC _{0-inf} (μg/mL/min)	423	304	511
Vd (L/kg)	0.91	1.18	1.3
BAV (%)	40	100	100

^a Compound dose for rat: iv and po at 15 mg/kg (10% DMSO/10% cyclodextrin in PBS). ^b Compound dose for dog: iv at 2.5 mg/kg (10% DMSO/10% cyclodextrin in PBS) and po at 10 mg/kg (methylcellulose vehicle).

which illustrates that by the use of this method compounds can be ranked in relative terms to provide an indication of oral exposure. A doubling in exposure at 60 min is seen for *N*-phenyl **34**, which is over and above that for 2-pyrimidinyl **27**, although poor solubility (0.001 mg/mL) prevented the further advancement of this compound. In contrast, 2- and 3-tetrahydrofurylamides **50** and **51** had enhanced water solubility, but their corresponding exposure levels were relatively poor. The cyclopropylamide, compound **47**, showed the greatest levels of absorption by the use of this limited time-point assay. This compound, along with ethylamide compound **46**, which also showed good potency in enzyme-free and cellular PF₅₀ assays, was advanced to further PK analysis.

Pharmacokinetic Profiles

To establish whether one of these compounds (**46** or **47**) had the right PK profile to warrant its selection as an orally bioavailable candidate for clinical use, we initially evaluated both compounds for oral bioavailability and pharmacokinetic stability in rats (Table 7). Despite these compounds being structurally comparable and profiling very similarly in terms of their rat iv PK values, cyclopropyl compound **47** showed a significantly greater oral exposure than did compound **46**, which confirms the mouse data. Accordingly, compound **47** was advanced to further pharmacokinetic analysis in dogs. Table 7 highlights the PK profile of **47** in dog following its dosing iv at 2.5 mg/kg and po at 10 mg/kg in a methylcellulose vehicle as a suspension formulation. The data show that this compound retains an excellent level of bioavailability that is similar to that seen in rat but has a lower relative clearance that equates to approximately 16% hepatic blood flow (68% in rat). As such, this pharmacokinetic profile provided therapeutically relevant levels of PARP inhibitor over at least 4 h in this species. Cyclopropylamide analog **47** was shown to possess good exposure together with attributes of potency and physicochemistry such that this compound was advanced to further analysis

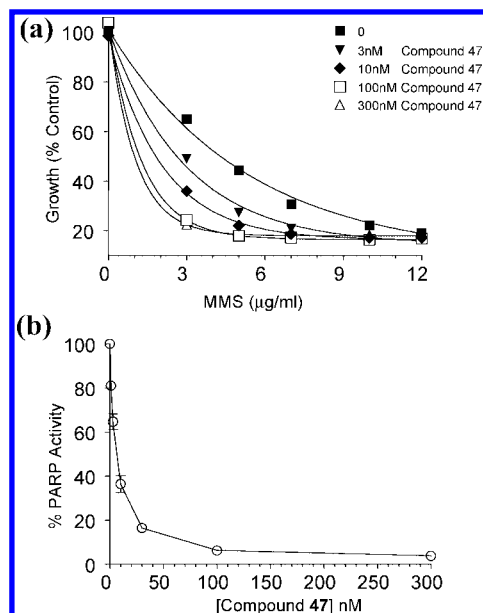


Figure 2. (a) Potentiation of methyl methanesulphonate (MMS) cell killing of cultured SW620 cells in combination with compound **47**. Increasing concentrations of MMS were coincubated with or without the PARP inhibitor at single concentrations ranging from 1 to 300 nM. (b) PARP activity in SW620 tumor cell lysates treated with increasing nM concentrations of compound **47**. PARP activity was quantified by the use of a PAR formation assay. (See the Experimental Section.)

of its cellular potency and in vivo efficacy to identify it as a potential clinical candidate.

In Vitro Cellular Potency

The cellular potency of **47** was evaluated in a number of in vitro models. Initial studies identified **47** as an effective agent to potentiate the cell killing by alkylating agent MMS. Following the establishment of a growth-inhibition curve for MMS on SW620 cells, the addition of the PARP-1 inhibitor at nM concentrations dose dependently increased the effectiveness of MMS (Figure 2a). The level of potentiation was seen to plateau around 100 nM concentration, which indicates that the maximal cellular activity for **47** in combination with MMS lies within this range. We confirmed this by directly measuring PARP-1 inhibitory activity in cells by using a PAR formation assay in which **47** was applied to SW620 cell lysates at a similar concentration range and identified the IC_{50} for PARP-1 inhibition to be around 6 nM and the total ablation of PARP-1 activity to be at concentrations of 30–100 nM (Figure 2b).

Consistent with previous data,²⁴ *BRCA1*-deficient cell lines MDA-MB-463 and HCC1937 were hypersensitive to PARP inhibition by compound **47** in comparison with *BRCA1*- and *BRCA2*-proficient cells (Figure 3). Consequently, the clinical use of compound **47** is being explored in *BRCA*-deficient tumors.³⁵

In Vivo Efficacy

On the basis of our in vitro cell data, the ability of compound **47** to potentiate the antitumor activity of the methylating chemotherapeutic agent, TMZ, was evaluated in an SW620 tumor model.

Animals bearing SW620 xenografted tumors were treated with compound **47** (10 mg/kg, po) in combination with TMZ (50 mg/kg, po) once daily for 5 consecutive days, after which the tumors were left to grow out. A considerable inhibition of tumor volumes as compared with that of the TMZ alone group

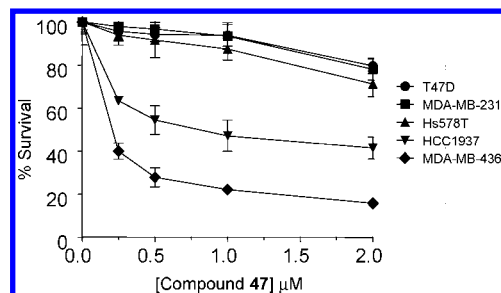


Figure 3. Cell survival (measured as a survival fraction) of breast cancer cell lines treated with PARP inhibitor **47**. The *BRCA1*- and *BRCA2*-proficient lines were Hs578T, MDA-MB-231, and T47D, whereas the *BRCA1*-deficient lines were MDA-MB-436 and HCC1937.

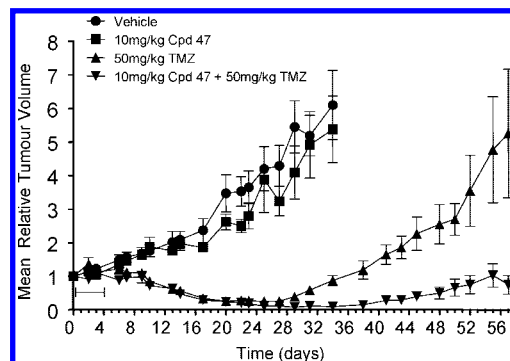


Figure 4. Antitumor efficacy of compound **47** in combination with temozolomide (TMZ) in an SW620 tumor model. Mice were orally dosed once daily for 5 consecutive days (days 0–4 are indicated by a short line), and compound **47** was administered 45 min before TMZ. Tumor volumes are shown relative to the initial tumor volume prior to dosing. Error bars represent SEM.

was observed for the TMZ plus compound **47** combination (mean values given as relative tumor volumes (RTV), Figure 4). This equated to over 80% tumor growth inhibition throughout the entire terminal phase of the study between TMZ treatment and the combination. The time to reach 2× RTVs for TMZ and combination treatment was 44 and 70 days, respectively (59% increase in latency). Higher RTV values such as 4× RTV (two doublings) could not be comparably assessed because tumors that were treated with the combination treatment did not attain this size during the duration of the study, which clearly demonstrates the pronounced potentiation of TMZ activity by compound **47** (Figure 4). TMZ was well tolerated with a maximum mean body weight loss of 6% on day 7 (3 days after dosing concluded) and full recovery within a week. Likewise, when administered in combination, the PARP inhibitor did not exacerbate the systemic toxicity of TMZ, with a maximum mean body weight loss of 9% on day 6 with full recovery of body weight within 3 days and with no mortalities (>20% weight loss), which signifies that the combination therapy was well tolerated under this dosing regimen.

Conclusions

The optimization of a series of substituted 4-benzyl-2*H*-phthalazin-1-ones has led to the identification of an array of highly potent PARP-1 inhibitors that possess cellular potency. Through a combination of parallel synthesis and subtle side-chain modification, compounds from both a homopiperazine and a piperazine series have been elaborated to introduce good oral bioavailability. Furthermore the introduction of a C-4 fluorine onto the benzyl linker has been shown to improve PF_{50} over

the corresponding des-fluoro analogs consistently. A medium throughput murine pharmacokinetic model was exploited to highlight key compounds for a more extensive analysis, and this approach led to the identification of **47**. Further preclinical profiling of **47** in cell lines with genetic lesions in the HR-repair pathway (BRCA1 and 2), together with in vivo activity in combination with the DNA-damaging agent TMZ, resulted in the selection of **47** for clinical development. Compound **47** (KU-0059436, AZD2281) is currently undergoing phase II clinical trials as a monotherapy in BRCA-deficient breast or ovarian cancer patients and in combination with selected cytotoxic agents over a range of tumors.

Experimental Section

All experiments were carried out under an inert atmosphere and at room temperature, unless otherwise stated. The purities of compounds for biological testing were assessed by one of two analytical LC-MS methods. The first method utilized a Spectra System P4000 pump and a Jones Genesis C18 column (4 μ m, 50 \times 4.6 mm²). Mobile phases A (0.1% formic acid in water) and B (acetonitrile) were used in a gradient of 5% B for 1 min, which rose to 98% B after 5 min, and were held for 3 min at a flow rate of 2 mL/min. Detection was by a TSP UV 6000LP detector at 254 nm UV and a 210–600 nm range PDA. We used a Finnigan LCQ mass spectrometer operating in positive-ion electrospray mode. The second method utilized an Agilent 1100 apparatus, Waters Alliance HT (2790 and 2795) equipment, or an HP1100 pump and diode array with a CTC autosampler run on a Phenomenex Gemini C18 column (5 mm, 50 \times 2 mm²) eluting with acidic eluant. (For example, by the use of a gradient, over 4 min, between 0 and 95% water/acetonitrile with 5% of 1% formic acid in 50:50 water/acetonitrile (v/v) mixture the MS component comprised a Waters ZQ mass spectrometer that scanned over an appropriate mass range.) Chromatograms for electrospray ionization (ESI) positive and negative base peak intensity and a UV total absorption chromatogram from 220–300 nm were generated, and values for *m/z* are given; generally, only ions that indicate the parent mass are reported, and unless otherwise stated, the value quoted is (M + H)⁺ for positive-ion mode and (M – H)[–] for negative-ion mode.

We conducted purification by preparative HPLC/MS on a Waters mass-directed purification system by utilizing a Waters 600 LC pump, a Waters Xterra C18 column (5 μ m, 19 \times 50 mm²), and a Micromass ZQ mass spectrometer operating in positive-ion ESI mode. Mobile phases A (0.1% formic acid in water) and B (0.1% formic acid in acetonitrile) were used in a gradient (5% B to 100% over 7 min; held for 3 min at a flow rate of 20 mL/min). The separation of the drug standards and their metabolites was carried out by the use of a Gemini C18 column (5 μ m, 250 \times 2 mm² i.d.) (Phenomenex, Macclesfield, U.K.). The column was heated to 50 °C, and the mobile-phase flow rate was 300 μ L/min. For all separations eluant A was 10 mM aqueous ammonium acetate. Eluant B was 10 mM ammonium acetate in methanol. (All chemicals and solvents were obtained from Fisher Scientific, Loughborough, U.K.) Each sample (10 μ L) was injected and subjected to the following mobile phase. We used an HPLC system that comprised the following parts: an autosampler (CTC Analytics), an HTS PAL apparatus (Presearch), a Thermo Surveyor Plus MS pump and photodiode array detector (ThermoFisher Scientific), and a Thermo Surveyor Plus PDA (ThermoFisher Scientific). The photodiode array detector was scanned over a wavelength range of 190–350 nm. All results are shown at 300–305 nm.

¹H NMR and ¹³C NMR were recorded by the use of a Bruker DPX 300 spectrometer at 300 and 75 MHz, respectively. Chemical shifts were reported in parts per million (ppm) on the δ scale relative to tetramethylsilane internal standard, and peak multiplicities are expressed as follows: s, singlet; d, doublet; dd, doublet of doublets; t, triplet; br s, broad singlet; and m, multiplet. Unless otherwise stated, all samples were dissolved in DMSO-*d*₆. NMR and mass spectra were run on isolated intermediates and final products and were consistent with the proposed structures.

High-resolution mass spectrometry was carried out on a Thermo LTQ XL Orbitrap mass spectrometer fitted with an ESI source that was used for all analyses (ThermoFisher Scientific). The ESI source was operated in positive-ionization mode with the following source conditions: a capillary temperature of 275 °C; sheath, auxiliary, and sweep gas flows of 30, 3, and 5, respectively (arbitrary units); and needle, capillary, and tube lens voltages of 4000, 48, and 75 V, respectively. We used the mass spectrometer in a data-dependent mode by using the following scan cycle: (1) scan 1, full scan 100–800 amu; (2) scan 2, MS/MS scan of the most intense ion detected in scan 1; and (3) scan 3, MS/MS of the most intense ion detected in scan 2. All data were collected at 30K resolution for scan 1 (50% valley definition) and at 7.5K resolution for scan modes 2 and 3. Accurate mass measurement was maintained by the use of three solvent/gas background impurities as lock masses: butylbenzenesulfonamide (*m/z* 214.08963), diisooctyl phthalate (*m/z* 391.284286), and a siloxane adduct, [Si(CH₃)₂O]₈NH₄⁺ (*m/z* 610.184156).

3-[(4-Oxo-3H-phthalazin-1-yl)methyl]benzoic Acid (7). To a stirred suspension of **1** (51.0 g, 0.38 mol) and **2** (52.0 g, 0.39 mol) in ethyl propionate (200 mL) was added a solution of sodium methoxide in methanol (25% wt, 1.530 mol) over 40 min, and the temperature was maintained below 30 °C. The reaction was then heated under reflux for 1 h before it was diluted with methanol (100 mL) and further heated for 1 h. The mixture was cooled and concentrated in vacuo. Water (1 L) was added to the resulting suspension, which was filtered. The filtrate was washed with diethyl ether (3 \times 200 mL) and was acidified with acetic acid (110 mL), and the suspension was stirred for 15 min. The product was collected by filtration, washed with water (100 mL), and dried in air to produce 69.2 g of 3-(1,3-dioxindene-2-yl)benzonitrile **3** (94%) as a red solid (95% purity by HPLC, material used without further purification). A suspension of **3** (48.3 g, 0.194 mol) in aqueous NaOH (39.1 g, 0.98 mol) in water (350 mL) was heated to 100 °C for 72 h. The solution was cooled to 20 °C and was acidified with HCl (2 N) to pH 2. After 15 min, the solid was filtered and was washed with water (3 \times 300 mL), hexane (2 \times 200 mL), and diethyl ether (2 \times 150 mL) and was dried to yield a pale-pink powder. The powder was suspended in hydrazine hydrate (250 mL, 5.0 mol) and was heated to 100 °C for 3 h. The reaction was cooled to 20 °C and was filtered. The filtrate was diluted with saturated aqueous NaHCO₃ solution (50 mL), was washed with ethyl acetate (2 \times 100 mL), and was acidified with 6 N HCl (ca. 75 mL) to pH 4. The resulting pale-yellow suspension was stirred for 10 min, and the product was collected by filtration and was washed with water (4 \times 150 mL), hexane (3 \times 200 mL), diethyl ether (2 \times 100 mL), and acetone (2 \times 100 mL) to produce 27.7 g of **7** (55%) as an off-white powder.

2-Fluoro-5-[(4-oxo-3H-phthalazin-1-yl)methyl]benzoic Acid (8). Dimethylphosphite (97.3 mL, 1.06 mol) was added dropwise to a solution of sodium methoxide (463 g, 1.14 mol) in methanol (1 L) at 0 °C. 2-Carboxybenzaldehyde (135 g, 0.90 mol) was then added portionwise to the reaction mixture over 20 min, and the temperature was maintained below 5 °C. The resulting orange solution was warmed to 20 °C over 2 h. Methanesulphonic acid (81.6 mL, 1.26 mol) was added to the reaction dropwise over 35 min, and the resulting white suspension was evaporated in vacuo. The white residue was treated with water (550 mL) and was extracted with DCM (3 \times 400 mL). The combined organic extracts were backwashed with water (2 \times 100 mL), were dried over MgSO₄, and were evaporated in vacuo to produce 194.0 g of 3-dimethoxyphosphoryl-3H-2-benzofuran-1-one **4** (89%) as a crystalline white solid. The material was carried forward without further purification. To a mixture of **4** (35.0 g, 0.14 mol) and 2-fluoro-5-formylbenzonitrile **5** (20.9 g, 0.14 mol) in THF (330 mL) was added triethylamine (14.0 mL, 0.14 mol) dropwise over 25 min, and the temperature was maintained below 15 °C. The reaction mixture was slowly warmed to 20 °C over 1 h and was then concentrated in vacuo. The residue was slurried in water (250 mL) for 30 min, and the solid was collected by filtration, was washed with water (2 \times 30 mL), hexane (2 \times 30 mL), and diethyl ether (2 \times 30 mL),

and was dried to produce 37.2 g of 2-fluoro-5-[(*Z/E*)-(3-oxo-2-benzofuran-1-ylidene)methyl]benzonitrile **6** (96%) as a 75:25 mixture of *E* and *Z* isomers. The material was carried forward without separation of the isomers. As such, to a stirred suspension of **6** (37.2 g, 0.14 mol) in water (200 mL) was added aqueous NaOH (13 N, 50 mL) with subsequent heating to 90 °C for 1 h. The reaction mixture was partially cooled to 70 °C and hydrazine hydrate (100 mL, 2.0 mol) added, and the mixture was stirred for 18 h at 70 °C. The reaction was cooled to ambient temperature and was acidified with HCl (8 N, ca. 80 mL) to pH 4. After 10 min, the suspension was filtered and was washed with water (2 × 60 mL), followed by diethyl ether (3 × 50 mL) and was dried to produce 30.1 g of **8** (77%) as a white powder.

tert-Butyl 4-[3-[(4-Oxo-3H-phthalazin-1-yl)methyl]benzoyl]piperazine-1-carboxylate (9). To a solution of **7** (5.0 g, 0.178 mol), *tert*-butyl-1-piperazine carboxylate (3.65 g, 0.196 mol), HBTU (6.82 g, 0.19 mol), and DIPEA (6.1 mL, 0.38 mol) were added to DMA (60 mL), and the mixture was stirred for 1 h. Water (100 mL) was added to the mixture, which was further stirred 1 h. The suspension was cooled to room temperature, was filtered, was washed with ice water (2 × 15 mL) and diethyl ether (2 × 15 mL), and was dried to produce 7.3 g of **9** (91%) as a white crystalline solid.

tert-Butyl 4-[3-[(4-Oxo-3H-phthalazin-1-yl)methyl]benzoyl]-1,4-diazepane-1-carboxylate (10). A solution of **7** (0.56 g, 2.0 mmol), *tert*-butyl-1-homopiperazine carboxylate (0.48 g, 2.4 mmol), HBTU (0.985 g, 2.60 mmol), and triethylamine (0.61 mL, 4.4 mmol) in DMF (3.5 mL) was stirred at ambient temperature for 18 h. Water (5 mL) was added in one portion, and the mixture was cooled (5 °C) for 1 h. The suspension was filtered, was washed with DMF–H₂O (1:1) (2 × 2 mL) and ether (2 × 2 mL), and was dried to produce 891 mg of **10** (97%) as a white solid.

tert-Butyl 4-[2-Fluoro-5-[(4-oxo-3H-phthalazin-1-yl)methyl]benzoyl]piperazine-1-carboxylate (11). To **8** (8.9 g, 30.0 mmol), *tert*-butyl-1-homopiperazine carboxylate (6.70 g, 36.0 mmol), HBTU (13.6 g, 36.0 mmol), and triethylamine (8.3 mL, 60.0 mmol) was added DMF (60 mL), and the mixture was stirred for 2 h. Water (60 mL) was added, and the mixture was cooled to 5 °C for >1 h. The suspension was filtered, was washed with ice-cold DMF–H₂O (1:1) (2 × 20 mL), ice-cold water (2 × 20 mL), cold IPA (2 × 20 mL), and cold diethyl ether (2 × 20 mL), and was dried to produce 13.6 g of **11** (96%) as a white solid.

tert-Butyl 4-[3-[(4-Oxo-3H-phthalazin-1-yl)methyl]benzoyl]-1,4-diazepane-1-carboxylate (12). A solution of **8** (1.50 g, 5.0 mmol), *tert*-butyl-1-homopiperazine carboxylate (1.20 g, 6.0 mmol), HBTU (2.64 g, 6.5 mmol), and triethylamine (1.5 mL, 11.0 mmol) in DMF (10 mL) was stirred at room temperature for 2 h. Water (10 mL) was added, and the mixture was cooled to 5 °C over 1 h. The suspension was filtered, was washed with ice-cold DMF–H₂O (1:1) (2 × 5 mL), cold water (2 × 5 mL), cold IPA (2 × 5 mL), and cold ether (2 × 5 mL), and was dried to yield 2.4 g of **12** (97%) as a cream solid.

4-[3-[(1,4-Diazepane-1-carbonyl)-phenyl]methyl]-2H-phthalazin-1-one (10a). To a cold (5 °C) solution of **10** (0.50 g, 1.08 mmol) in DCM (10 mL) was added dropwise TFA (2 mL, 10.8 mmol). After 2 h, the reaction was reduced to dryness in vacuo and was resuspended in DCM (10 mL). Triethylamine (ca. 0.5 mL) was added dropwise. The mixture was then absorbed onto silica gel and was subjected to SiO₂ chromatography with EtOAc/MeOH (7:1) as the eluant to afford 0.33 g of **10a** (83%) as a white solid.

4-[3-[(1,4-Diazepane-1-carbonyl)-4-fluorophenyl]methyl]-2H-phthalazin-1-one (14). HCl (6 N, 10 mL) was added dropwise to a solution of **12** (2.40 g, 5 mmol) in ethanol (5 mL). The reaction was stirred for 3 h and was then concentrated in vacuo (ca. 5 mL). The pH of the mixture was adjusted to 10 by the use of aqueous NH₃OH. The mixture was then extracted with DCM (3 × 20 mL), and combined extracts were washed with water (1 × 20 mL) and were dried over Na₂SO₄. After the mixture stood overnight, **14** was isolated by filtration (1.25 g, 66%) as a white crystalline solid (99% purity by HPLC). ¹H NMR (DMSO-*d*₆, δ): 12.58 (s, 1H), 8.28–8.19 (m, 1H), 8.04–7.72 (m, 3H), 7.51–7.10 (m, 3H), 4.31 (s, 2H), 3.81–3.54 (m, 2H), 3.39–2.64 (m, 7H), 2.04–1.55 (m,

2H). FTMS + PESI *m/z*: calcd for C₂₁H₂₂FN₄O₃, 381.172130; found, 381.17303.

Method Used to Prepare 15 and 17. **4-[3-[(4-(2-Hydroxyethyl)-1,4-diazepane-1-carbonyl]phenyl]methyl]-2H-phthalazin-1-one (15).** To a solution of **7** (67 mg, 0.24 mmol), DIPEA (0.7 mL, 4.0 mmol), and HBTU (95 mg, 0.25 mmol) in DMA (1 mL) at ambient temperature was added a solution of 2-[1,4]diazepan-1-ylethanol (0.26 mmol) in DMA (0.5 mL). The reaction mixture was stirred at room temperature for 16 h and was then submitted for preparative HPLC purification to produce **15**.

A similar procedure was used to prepare compound **17**.

Method Used to Prepare 16 and 21. **4-[4-Fluoro-3-[(4-(2-hydroxyethyl)-1,4-diazepane-1-carbonyl]phenyl]methyl]-2H-phthalazin-1-one (16).** To a solution of **8** (50 mg, 0.171 mmol), DIPEA (0.6 mL, 3.4 mmol), and HBTU (71 mg, 0.19 mmol) in DMA (1 mL) at ambient temperature was added an appropriate solution of 2-[1,4]diazepan-1-ylethanol (0.19 mmol) in DMA (0.5 mL). The reaction mixture was stirred at room temperature for 16 h and was then submitted for preparative HPLC purification: ¹H NMR (DMSO-*d*₆, δ): 12.58 (s, 1H), 8.33–8.21 (m, 1H), 7.98–7.75 (m, 3H), 7.52–7.16 (m, 3H), 4.68 (d, *J* = 6.1 Hz, 1H), 4.33 (s, 2H), 4.06–3.87 (m, 2H), 3.80–3.63 (m, 2H), 3.63–3.31 (m, 2H), 3.00–2.88 (m, 2H), 2.88–2.75 (m, 3H), 2.10–1.90 (m, 1H), 1.82–1.73 (m, 2H). FTMS + PESI *m/z*: calcd for C₂₃H₂₆FN₄O₃, 425.19834; found, 425.19755.

A similar procedure was used to prepare compound **21**.

4-[3-[(4-Ethylsulfonyl)-1,4-diazepane-1-carbonyl]phenyl]methyl]-2H-phthalazin-1-one (18). To a solution of **10a** (72 mg, 0.200 mmol) and triethylamine (41 μL, 0.3 mmol) in dry DCM (1 mL) was added ethane sulfonyl chloride (29 mg, 0.23 mmol). The mixture was stirred at ambient temperature for 4 h and was then quenched by the addition of water (0.5 mL). The crude mixture was then purified by preparative HPLC purification: ¹H NMR (DMSO-*d*₆, δ): 12.58 (s, 1H), 8.34–8.20 (m, 1H), 8.02–7.75 (m, 3H), 7.49–7.15 (m, 4H), 4.35 (s, 2H), 3.77–3.58 (m, 2H), 3.53–3.21 (m, 5H), 3.16–2.97 (m, 2H), 1.82 (s, 1H), 1.50 (s, 1H), 1.26–1.11 (m, 3H). FTMS + PESI *m/z*: calcd for C₂₃H₂₇N₄O₄S, 455.17475; found, 455.17376.

4-[3-[(4-(Morpholine-4-carbonyl)-1,4-diazepane-1-carbonyl]phenyl]methyl]-2H-phthalazin-1-one (19). To a solution of **10a** (72 mg, 0.200 mmol) and Et₃N (33 μL, 0.24 mmol) in dry DCM (1 mL) was added 4-morpholinecarbonyl chloride (33 mg, 0.240 mmol). The mixture was stirred at ambient temperature for 10 h and was quenched by the addition of methanol (0.5 mL). The crude mixture was then purified by preparative HPLC purification to produce **19**.

4-[4-Fluoro-3-[(4-(morpholine-4-carbonyl)-1,4-diazepane-1-carbonyl]phenyl]methyl]-2H-phthalazin-1-one (20). To a solution of **14** (38 mg, 0.100 mmol) and triethylamine (33 μL, 0.24 mmol) in dry DCM (1 mL) was added 4-morpholinecarbonyl chloride (15 mg, 0.11 mmol). The mixture was stirred at ambient temperature for 4 h and was then quenched by the addition of methanol (0.5 mL). The crude product was then purified by preparative HPLC: ¹H NMR (300 MHz, DMSO-*d*₆, δ): 12.56 (s, 1H), 8.33–8.19 (m, 1H), 8.02–7.77 (m, 3H), 7.46–7.35 (m, 1H), 7.31 (dd, *J* = 6.4, 2.2 Hz, 1H), 7.27–7.15 (m, 1H), 4.32 (s, 2H), 3.82–3.40 (m, 8H), 3.37–3.16 (m, 6H), 3.12–2.95 (m, 4H). FTMS + PESI *m/z*: calcd for C₂₆H₂₉FN₅O₄, 494.21980; found, 494.21828.

4-[3-[(4-(Cyclopropanecarbonyl)-1,4-diazepane-1-carbonyl)-4-fluorophenyl]methyl]-2H-phthalazin-1-one (22). To a solution of **14** (38 mg, 0.100 mmol) and Et₃N (33 μL, 0.24 mmol) in dry DCM (1 mL) was added cyclopropanecarbonyl chloride (11 mg, 0.11 mmol). The mixture was stirred at ambient temperature for 8 h and was then quenched by addition of methanol (0.5 mL). The crude product was then purified by preparative HPLC: ¹H NMR (300 MHz, DMSO-*d*₆, δ): 12.56 (s, 1H), 8.26 (d, *J* = 7.7 Hz, 1H), 8.04–7.77 (m, 3H), 7.49–7.29 (m, 1H), 7.29–7.14 (m, 2H), 4.32 (s, 2H), 3.83 (m, 1H), 3.73–3.54 (m, 3H), 3.43 (m, 2H), 3.26 (m, 4H), 1.55–1.28 (m, 1H), 0.70 (m, 4H). FTMS + PESI *m/z*: calcd for C₂₅H₂₆FN₄O₃, 449.19834; found, 449.19752.

4-[[3-(Piperazine-1-carbonyl)phenyl]methyl]-2H-phthalazin-1-one (23). To a cold (5 °C) solution of **9** (5.3 g, 11.9 mmol) in DCM (60 mL) was added dropwise TFA (8 mL, 108 mmol). After 2 h, the reaction was reduced to dryness in vacuo and was resuspended in DCM (60 mL). Triethylamine (ca. 3 mL, 21 mmol) was added dropwise. The mixture was then absorbed onto silica gel and was subjected to SiO₂ chromatography with the eluant EtOAc/MeOH (7:1) to afford 3.85 g of **23** (92%) as a white solid (99% purity by HPLC).

4-[[4-Fluoro-3-(piperazine-1-carbonyl)phenyl]methyl]-2H-phthalazin-1-one (24). HCl (6 N, 60 mL) was added to a solution of **11** (13.6 g, 29 mmol) in EtOH (30 mL) at room temperature. The reaction was stirred for 3 h and was then concentrated in vacuo (ca. 50 mL). The pH of the mixture was adjusted to 10 by the use of aqueous ammonium hydroxide (4 N). The mixture was then extracted with DCM (3 × 50 mL), and combined extracts were washed with water (50 mL) and were dried over Na₂SO₄. After the mixture stood overnight, **24** was isolated by filtration (9.9 g, 92%) as a white crystalline solid (99% purity by HPLC).

General Method Used to Prepare 25, 27, 33, 35, 37, and 39. **4-[[3-(4-Pyridin-2-ylpiperazine-1-carbonyl)phenyl]methyl]-2H-phthalazin-1-one (25).** To a solution of **7** (48 mg, 0.171 mmol) in DMA (1 mL) were added DIPEA (0.6 mL, 3.4 mmol) and HBTU (71 mg, 0.188 mmol), followed by an appropriate solution of pyridine-2-ylamine (0.188 mmol) in DMA (0.5 mL). The reaction mixture was stirred at room temperature for 16 h and was then submitted for preparative HPLC purification to produce **25**. ¹H NMR (DMSO-*d*₆, δ): 12.58 (s, 1H), 8.27 (dd, *J* = 0.9, 7.5 Hz, 1H), 8.13 (dd, *J* = 1.2, 4.8 Hz, 1H), 7.98 (m, 1H), 7.86 (m, 2H), 7.56 (m, 1H), 7.40 (m, 3H), 7.27 (m, 1H), 6.82 (d, *J* = 8.7 Hz, 1H), 6.67 (dd, *J* = 5.1, 1.5 Hz, 1H), 4.37 (s, 2H), 3.31 (m, 8H). FTMS + PESI *m/z*: calcd for C₂₅H₂₄N₅O₂, 426.19245; found, 426.19151.

A similar procedure was used to prepare compounds **27**, **33**, **35**, **37**, and **39**.

4-[[3-(4-Ethylsulfonylpiperazine-1-carbonyl)phenyl]methyl]-2H-phthalazin-1-one (29). To a solution of **23** (45 mg, 0.072 mmol) in dry DCM (11 mL) were added DIPEA (25 μL, 0.146 mmol) and ethanesulfonyl chloride (7 μL, 0.075 mmol). The reaction mixture was stirred at room temperature for 16 h and was then submitted for preparative HPLC purification to produce **29**.

4-[[3-(4-Ethylsulfonylpiperazine-1-carbonyl)-4-fluorophenyl]methyl]-2H-phthalazin-1-one (30). To a solution of **24** (25 mg, 0.072 mmol) in dry DCM (1 mL) were added DIPEA (25 μL, 0.146 mmol) and ethanesulfonyl chloride (7 μL, 0.075 mmol). The reaction mixture was stirred at room temperature for 16 h and was then submitted for preparative HPLC purification. ¹H NMR (DMSO-*d*₆, δ): 12.58 (s, 1H), 8.27 (dd, *J* = 7.2, 1.5 Hz, 1H), 7.95 (dd, *J* = 7.2, 1.5 Hz, 1H), 7.92–7.79 (m, 2H), 7.49–7.41 (m, 1H), 7.36 (dd, *J* = 6.5, 2.2 Hz, 1H), 7.24 (t, *J* = 9.6 Hz, 1H), 4.34 (s, 2H), 3.70 (s, 2H), 3.25 (t, *J* = 4.5 Hz, 4H), 3.11–3.02 (m, 4H), 1.21 (t, *J* = 7.2 Hz, 3H). FTMS + PESI *m/z*: calcd for C₂₂H₂₄FN₄O₄S, 459.14968; found, 459.14877.

4-[[3-[4-(Morpholine-4-carbonyl)piperazine-1-carbonyl]phenyl]methyl]-2H-phthalazin-1-one (31). To a solution of **23** (25 mg, 0.072 mmol) in dry DCM (1 mL) were added DIPEA (25 μL, 0.15 mmol) and morpholine-4-carbonyl chloride (12 mg, 0.075 mmol). The reaction mixture was stirred at room temperature for 16 h and was then submitted for preparative HPLC purification to produce **31**.

4-[[4-Fluoro-3-[4-(morpholine-4-carbonyl)piperazine-1-carbonyl]phenyl]methyl]-2H-phthalazin-1-one (32). To a solution of **24** (25 mg, 0.072 mmol) in dry DCM (1 mL) were added DIPEA (25 μL, 0.146 mmol) and morpholine-4-carbonyl chloride (12 mg, 0.075 mmol). The reaction mixture was stirred at room temperature for 8 h and was then submitted for preparative HPLC purification. ¹H NMR (DMSO-*d*₆, δ): 12.58 (s, 1H), 8.34–8.20 (m, H), 8.03–7.75 (m, 3H), 7.49–7.15 (m, 6H), 7.00–6.74 (m, 3H), 4.37 (s, 2H), 3.79–3.10 (m, 8H). FTMS + PESI *m/z*: calcd for C₂₅H₂₇FN₅O₄, 480.20415; found, 480.20294.

General Method Used to Prepare 42, 43, and 44. **4-[[4-Fluoro-3-(4-propylpiperazine-1-carbonyl)phenyl]methyl]-2H-phthalazin-1-one (42).** To a solution of **24** (50 mg, 0.144 mmol) in dry THF (2 mL) were added DIPEA (25 μL, 0.146 mmol) and the appropriate 1-bromopropane (0.075 mmol). The reaction mixture was heated at 50 °C for 16 h and was then submitted for preparative HPLC purification to produce **42**: ¹H NMR (DMSO-*d*₆, δ): 12.57 (s, 1H), 8.33–8.20 (m, 1H), 8.00–7.78 (m, 3H), 7.51–7.14 (m, 3H), 4.33 (s, 2H), 3.74–3.52 (m, 2H), 3.19 (s, 2H), 2.63–2.26 (m, 4H) 1.46 (dd, *J* = 14.9, 7.4 Hz, 2H), 0.86 (t, *J* = 7.4 Hz, 3H). FTMS + PESI *m/z*: calcd for C₂₃H₂₆FN₄O₂, 409.20343; found, 409.20230.

A similar procedure was used to prepare compounds **43** and **44**.

General Method Used to Prepare 26, 28, 34, 36, 38, 40, 41, and 45–51. **4-[[3-[4-(Cyclopropanecarbonyl)piperazine-1-carbonyl]-4-fluorophenyl]methyl]-2H-phthalazin-1-one (47).** To a solution of acid **7** (50 mg, 0.168 mmol) in DMA (1 mL) were added DIPEA (56 μL, 0.336 mmol) and HBTU (64 mg, 0.170 mmol), followed by cyclopropylpiperazine-1-ylmethanone (0.170 mmol). The reaction mixture was stirred at room temperature for 16 h and was then submitted for preparative HPLC purification to produce **47**: ¹H NMR (DMSO-*d*₆, δ): 12.57 (s, 1H), 8.27 (dd, *J* = 7.7, 1.2 Hz, 1H), 7.97 (dd, *J* = 7.7, 1.2 Hz, 1H), 7.94–7.78 (m, 2H), 7.49–7.40 (m, 1H), 7.42–7.34 (m, 1H), 7.24 (t, *J* = 9.0 Hz, 1H), 4.34 (s, 2H), 3.86–3.10 (m, 8H), 2.09–1.82 (m, 1H), 0.74 (m, 4H). FTMS + PESI *m/z*: calcd for C₂₄H₂₄FN₄O₃, 435.18269; found, 435.18199.

A similar procedure was used to prepare compounds **26**, **28**, **34**, **36**, **38**, **40**, **41**, **45**, **46**, and **48–51**.

Solubility Measurements. The thermodynamic solubility of a research compound is measured under standard conditions. A known amount of the compound is stirred in 0.1 M phosphate buffer (pH 7.4) at constant temperature (25 °C) for 24 h. The supernatant is then separated from the undissolved material by centrifugation and is subsequently analyzed and quantified against a standard of known concentration in DMSO by the use of generic HPLC–UV methodology coupled to mass spectral peak identification.

Pharmacokinetics. We carried out pharmacokinetics determinations in mouse, rat, and dog. All doses of the compounds were given as a single dose either intravenously (iv) or orally (po); see dose level, as described in Tables 6 and 7). For the iv studies, the compounds were formulated in a mixture of 10% DMSO/10% cyclodextrin in PBS. For the oral studies, the compounds were also predominantly formulated as a solution in 10% DMSO/10% cyclodextrin in PBS except for compound **47**, where a suspension in methylcellulose/PBS was used for oral dosing in dogs.

In Vitro Isolated Enzyme Assay. This assay determined the ability of test compounds to inhibit PARP-1 enzyme activity. The method that was used was as reported.⁴³ We measured PARP-2 activity inhibition by using a variation of the PARP-1 assay in which PARP-2 protein (recombinant) was bound down by a PARP-2 specific antibody in a 96-well white-walled plate. PARP-2 activity was measured following ³H–NAD⁺ DNA additions. After washing, scintillant was added to measure ³H-incorporated ribosylations. For tankyrase-1, an AlphaScreen (Perkin-Elmer) assay was developed in which HIS-tagged recombinant TANK-1 protein was incubated with biotinylated NAD⁺ in a 384-well ProxiPlate assay. Alpha beads were added to bind the HIS and biotin tags to create a proximity signal, whereas the inhibition of TANK-1 activity was directly proportional to the loss of this signal. All experiments were repeated at least three times.

In Vitro Cell PF₅₀ Assay. The PF₅₀ value is the potentiation factor, which is calculated as the ratio of the IC₅₀ of the control growth with alkylating agent methylmethane sulfonate (MMS) divided by the IC₅₀ of the MMS combined with the PARP inhibitor. HeLa B cells were used, and the test compounds were tested at a fixed 200 nM concentration for screening with MMS. For the testing of compound **47** on the SW620 colorectal cell line (Figure 2), the concentrations that were used were 1, 3, 10, 100 and 300 nM. Cell growth was assessed by the use of the sulforhodamine B (SRB) assay.⁴⁴

Ex Vivo PARP Activity Assay. SW620 whole-cell protein extracts were prepared by incubation in extraction buffer (1× PBS, 1% NP-40, protease inhibitor cocktail (Roche), 200 μ M DTT) for 10 min at 4 °C. PARP activity was determined by the quantification of the amount of PAR formation after ex vivo activation. PARP activation reactions were performed by the use of 65 ng of SW620 whole-cell extract in a reaction mix (50 mM Tris pH 8, 4 mM $MgCl_2$, 200 μ M DTT, 200 μ M NAD^+ , 20 ng/ μ L DNA) at 30 °C for 5 min. The amount of PAR that formed in each reaction was then quantified by the use of the Meso Scale Discovery assay platform. Data were calculated from triplicate experiments as the mean percentage of PARP activity relative to vehicle controls \pm SE and IC_{50} , which were calculated by the use of XL-FIT 4 software.

Cell Lines and Culture. SW620 colon, A2780 ovarian, HCC1937, Hs578T, MDA-MB-231, MDA-MB-436, and T47D breast cancer cell lines were obtained from either ATCC or ECACC repositories. All cell lines were grown as monolayers in RPMI1640 medium that was supplemented with 10% v/v FBS, 100 μ g/mL penicillin, and 100 μ g/mL streptomycin.

Cell Line Cytotoxicity Assays. The effect of KU-0059436 on the cell survival of breast cancer cell lines was determined by the use of clonogenic assays, as previously described.⁴⁵ Briefly, cells were seeded in six-well plates and were left to attach overnight. Vehicle control (DMSO) or increasing concentrations of KU-0059436 (up to 4 μ M) were added to the cells, and the mixture was left for 7–14 days, depending on the cell type, before surviving colonies were counted. Data were calculated from triplicate wells as the mean percentage of cell survival relative to vehicle controls \pm SE and IC_{50} , which were calculated by the use of XL-FIT 4 software.

Potential of MMS Cytotoxicity by 47 Determined by the Use of Sulforhodamine B Cell Growth Assays. SW620 cells were seeded in 96-well plates and were left to attach overnight. Cells were preincubated with vehicle control (DMSO) or with a single concentration of KU-0059436 (1, 3, 10, 30, 100 or 300 nM) for 1 h before the addition of increasing concentrations of MMS. Cells were incubated in the presence of each drug combination for 4 days before cell growth was quantified by the use of an SRB assay.⁴⁴ Data were calculated from triplicate wells as the mean percentage of cell growth relative to KU-0059436-only wells, and \pm SE and IC_{50} were calculated by the use of XL-FIT 4 software. SW620 cells showed <24% growth inhibition (>76% cell growth) when only KU-0059436 was used at concentrations below 300 nM (data not shown).

Mouse Xenografts. Tagged mice were inoculated sc with 5×10^6 cells in 0.1 mL of PBS to the right flank. Tumors were measured thrice weekly, and tumor volumes were estimated from the formula $[\text{length}/2] \times [\text{width}^2]$. For xenograft chemopotential studies, established tumors in each animal were individually normalized to their size at the start of the experiment, and the data were calculated as the change in tumor volume relative to the day 0 volume by the use of the relative tumor volume (RTV) formula, $RTV = TV_x/TV_0$, where TV_x is the tumor volume on any day and TV_0 is the tumor volume at the initiation of dosing (i.e., day 0). In the tumor growth curves, the mean represents a full complement of animals in the treatment groups; below this threshold, we ceased plotting.

Dosing Regimen. When the mean tumor volume reached 100 mm³, tumor-bearing mice were randomized into treatment groups with eight animals in each group being dosed orally once daily for 5 consecutive days (po, q.d., $\times 5$); for the combination therapies, the PARP inhibitor was administered 45 min before TMZ. Compound 47 was formulated in solution, and TMZ was formulated as a homogeneous suspension in corn oil (Sigma); both dosing solutions were freshly made each day. Mice in the no-treatment group received both vehicles on a mg/kg basis. Mice were weighed daily during the dosing phase to calculate the day's dose and any signs of body weight loss accurately (20% weight loss led to the animal being euthanized). Statistical analyses were calculated on the data only when a full complement of animals was present in the treatment groups (i.e., day 13 for the vehicle and 47 monotherapy groups and day 45 for the TMZ and combination

comparisons). From the Jonckheere–Terpstra trend test, we concluded that at day 45 there was a statistically significant effect of increasing the dose of 47 (10 mg/kg, data shown only in Figure 3) when used in combination with 50 mg/kg TMZ as compared with that of TMZ alone ($p < 0.0001$). This was confirmed by the use of Wilcoxon rank-sum tests, which compared the combination treatment groups versus TMZ alone to demonstrate statistically significant differences between TMZ monotherapy and TMZ in combination with 47 at 10 mg/kg ($p = 0.007$) at day 45.

Acknowledgment. We acknowledge the invaluable technical assistance of the following: Adrian Moore, Penny Wright, James Pullen, Barry Pope, David Rudge, Nicholas Barron, Craig Roberts, Jon Eden, Carlos Fernandez Lence, Joanne Gibney, Kristel Blackburn, Alexandra Fundo, and Rachael Tuppin. Also, we thank Madeleine Vickers (Structure Purity Group, Astra-Zeneca) for all high-resolution mass spectroscopy determination, Elizabeth Mills (Statistical Sciences Group, Discovery, Astra-Zeneca) for statistical analysis conducted on the in vivo experimentation, and Nicola Griffin for help with the manuscript.

Supporting Information Available: High-resolution mass spectra and HPLC purity data for all target compounds and additional spectroscopic and purity data for intermediates 4, 6–9, 10, 10a, 11, and 12 and target compounds 15, 17, 19, 21, 23, 24, 26–29, 31, 33–41, 43–46, and 48–51. This material is available free of charge via the Internet at <http://pubs.acs.org>.

References

- (1) D'Amours, D.; Desnoyers, S.; D'Silva, I.; Poirier, G. G. Poly(ADP-ribose)ylation reactions in the regulation of nuclear functions. *Biochem. J.* **1999**, *342*, 249–268.
- (2) d'Adda di Fagagna, F.; Hande, M. P.; Tong, W. M.; Lansdorp, P. M.; Wang, Z. Q.; Jackson, S. P. Functions of poly(ADP-ribose) polymerase in controlling telomere length and chromosomal stability. *Nat. Genet.* **1999**, *23*, 76–80.
- (3) Virag, L.; Szabo, C. The therapeutic potential of poly(ADP-ribose) polymerase inhibitors. *Pharmacol. Rev.* **2002**, *54*, 375–429.
- (4) Ame, J. C.; Spenlehauer, C.; de Murcia, G. The PARP superfamily. *BioEssays* **2004**, *26*, 882–893.
- (5) Diefenbach, J.; Burkle, A. Introduction to poly(ADP-ribose) metabolism. *Cell. Mol. Life Sci.* **2005**, *62*, 721–730.
- (6) Huber, A.; Bai, P.; de Murcia, J. M.; de Murcia, G. PARP-1, PARP-2, and ATM in the DNA damage response: functional synergy in mouse development. *DNA Repair* **2004**, *3*, 1103–1108.
- (7) Kickhoefer, V. A.; Siva, A. C.; Kederasha, N. L.; Inman, E. M.; Ruland, C.; Streuli, M.; Rome, L. H. The 193-kD vault protein, VPARP, is a novel poly(ADP-ribose) polymerase. *J. Cell Biol.* **1999**, *146*, 917–928.
- (8) Smith, S.; Gariat, I.; Schmitt, A.; de Lange, T. Tankyrase, a poly(ADP-ribose) polymerase at human telomeres. *Science* **1998**, *282*, 1484–1487.
- (9) Althaus, F. R.; Richter, C. ADP-ribosylation of proteins. Enzymology and biological significance. *Mol. Biol., Biochem. Biophys.* **1987**, *37*, 1–237.
- (10) Le Rhun, Y.; Kirkland, J. B.; Shah, G. M. Cellular responses to DNA damage in the absence of poly(ADP-ribose) polymerase. *Biochem. Biophys. Res. Commun.* **1998**, *245*, 1–10.
- (11) Wang, Z. Q.; Auer, B.; Stingl, L.; Berghammer, H.; Haidacher, D.; Schweiger, M.; Wagner, E. F. Mice lacking ADPRT and poly(ADP-ribose)ylation develop normally but are susceptible to skin disease. *Genes Dev.* **1995**, *9*, 509–520.
- (12) Ménissier de Murcia, J.; Niedergang, C.; Trucco, C.; Ricoul, M.; Dutrillaux, B.; Mark, M.; Oliver, F. J.; Masson, M.; Dierich, A.; LeMeur, M.; Walzinger, C.; Chambon, P.; de Murcia, G. Requirement of poly(ADP-ribose) polymerase in recovery from DNA damage in mice and in cells. *Proc. Natl. Acad. Sci. U.S.A.* **1997**, *94*, 7303–7307.
- (13) Ben-Hur, E.; Utsumi, H.; Elkind, M. M. Inhibitors of poly(ADP-ribose) synthesis enhance radiation response by differentially affecting repair of potentially lethal versus sublethal damage. *Br. J. Cancer, Suppl.* **1984**, *6*, 39–42.
- (14) Schlicker, A.; Peschke, P.; Burkle, A.; Hahn, E. W.; Kim, J. H. 4-Amino-1,8-naphthalimide: a novel inhibitor of poly(ADP-ribose) polymerase and radiation sensitizer. *Int. J. Radiat. Biol.* **1999**, *75*, 91–100.

- (15) Durkacz, B. W.; Omidiji, O.; Gray, D. A.; Shall, S. (ADP-ribose)n participates in DNA excision repair. *Nature* **1980**, *283*, 593–596.
- (16) Berger, N. A. Poly(ADP-ribose) in the cellular response to DNA damage. *Radiat. Res.* **1985**, *101*, 4–14.
- (17) Jagtap, P.; Szabo, C. Poly(ADP-ribose) polymerase and the therapeutic effects of its inhibitors. *Nat. Rev. Drug Discovery* **2005**, *4*, 421–440.
- (18) De la Lastra, C. A.; Villegas, I.; Sanchez-Fidalgo, S. Poly(ADP-ribose) polymerase inhibitors: new pharmacological functions and potential clinical implications. *Curr. Pharm. Des.* **2007**, *13*, 933–962.
- (19) Delaney, C. A.; Wang, L.-Z.; Kyle, S.; White, A. W.; Calvert, H.; Curtin, N. J.; Durkacz, B. W.; Hostomsky, Z.; Newell, D. R. Potentiation of temozolomide and topotecan growth inhibition and cytotoxicity by novel poly(adenosine diphosphoribose) polymerase inhibitors in a panel of human tumor cell lines. *Clin. Cancer Res.* **2000**, *6*, 2860–2867.
- (20) Miknyoczki, S. J.; Jones-Bolin, S.; Pritchard, S.; Hunter, K.; Zhao, H.; Wan, W.; Ator, M.; Bihovsky, R.; Hudkins, R.; Chatterjee, S.; Klein-Szanto, A.; Dionne, C.; Ruggeri, B. Chemopotentiation of temozolomide, irinotecan, and cisplatin activity by CEP-6800, a poly(ADP-ribose) polymerase inhibitor. *Mol. Cancer Ther.* **2003**, *2*, 371–382.
- (21) Tentori, L.; Graziani, G. Chemopotentiation by PARP inhibitors in cancer therapy. *Pharmacol. Res.* **2005**, *52*, 25–33.
- (22) Narod, S. A.; Foulkes, W. D. BRCA1 and BRCA2: 1994 and beyond. *Nat. Rev. Cancer* **2004**, *4*, 665–676.
- (23) Bryant, H. E.; Schultz, N.; Thomas, H. D.; Parker, K. M.; Flower, D.; Lopez, E.; Kyle, S.; Meuth, M.; Curtin, N. J.; Helleday, T. Specific killing of BRCA2-deficient tumours with inhibitors of poly(ADP-ribose) polymerase. *Nature* **2005**, *434*, 913–917.
- (24) Farmer, H.; McCabe, N.; Lord, C. J.; Tutt, A. N. J.; Johnson, D. A.; Richardson, T. B.; Santarosa, M.; Dillon, K. J.; Hickson, I.; Knights, C.; Martin, N. M. B.; Jackson, S. P.; Smith, G. C. M.; Ashworth, A. Targeting the DNA repair defect in BRCA mutant cells as a therapeutic strategy. *Nature* **2005**, *434*, 917–921.
- (25) Jasin, M. Homologous repair of DNA damage and tumorigenesis: the BRCA connection. *Oncogene* **2002**, *21*, 8981–8993.
- (26) Tutt, A.; Ashworth, A. The relationship between the roles of BRCA genes in DNA repair and cancer predisposition. *Trends Mol. Med.* **2002**, *8*, 571–576.
- (27) Radice, P. Mutations of BRCA genes in hereditary breast and ovarian cancer. *J. Exp. Clin. Cancer Res.* **2002**, *21*, 9–12.
- (28) Hoeijmakers, J. H. Genome maintenance mechanisms for preventing cancer. *Nature* **2001**, *411*, 366–374.
- (29) Bernstein, C.; Bernstein, H.; Payne, C. M.; Garewal, H. DNA repair/pro-apoptotic dual-role proteins in five major DNA repair pathways: fail-safe protection against carcinogenesis. *Mutat. Res.* **2002**, *511*, 145–178.
- (30) Kennedy, R. D.; D'Andrea, A. D. DNA repair pathways in clinical practice: lessons from pediatric cancer susceptibility syndromes. *J. Clin. Oncol.* **2006**, *24*, 3799–3808.
- (31) Ratnam, K.; Low, J. A. Current development of clinical inhibitors of poly(ADP-ribose) polymerase in oncology. *Clin. Cancer Res.* **2007**, *13*, 1383–1388.
- (32) Thomas, H. D.; Calabrese, C. R.; Batey, M. A.; Canan, S.; Hostomsky, Z.; Kyle, S.; Maegley, K. A.; Newell, D. R.; Skaltzky, D.; Wang, L. Z.; Webber, S. E.; Curtin, N. J. Preclinical selection of a novel poly(ADP-ribose) polymerase inhibitor for clinical trial. *Mol. Cancer Ther.* **2007**, *6*, 945–956.
- (33) Mason, K. A.; Valdecana, D.; Hunter, N. R.; Milas, L. INO-1001, a novel inhibitor of poly(ADP-ribose) polymerase, enhances tumor response to doxorubicin. *Invest. New Drugs* **2008**, *26*, 1–5.
- (34) Donawho, C. K.; Luo, Y.; Luo, Y.; Penning, T. D.; Bauch, J. L.; Bouska, J. J.; Bontcheva-Diaz, V. D.; Cox, B. F.; DeWeese, T. L.; Dillehay, L. E.; Ferguson, D. C.; Ghoreishi-Haack, N. S.; Grimm, D. R.; Guan, R.; Han, E. K.; Holley-Shanks, R. R.; Hristov, B.; Idler, K. B.; Jarvis, K.; Johnson, E. F.; Kleinberg, L. R.; Klinghofer, V.; Lasko, L. M.; Liu, X.; Marsh, K. C.; McGonigal, T. P.; Meulbroek, J. A.; Olson, A. M.; Palma, J. P.; Rodriguez, L. E.; Shi, Y.; Stavropoulos, J. A.; Tsurutani, A. C.; Zhu, G. D.; Rosenberg, S. H.; Giranda, V. L.; Frost, D. J. ABT-888, an orally active poly(ADP-ribose) polymerase inhibitor that potentiates DNA-damaging agents in preclinical tumor models. *Clin. Cancer Res.* **2007**, *13*, 2728–2737.
- (35) Yap, T. A. First in human phase I pharmacokinetic (PK) and pharmacodynamic (PD) study of KU-0059436 (Ku), a small molecule inhibitor of poly ADP-ribose polymerase (PARP) in cancer patients (p), including BRCA1/2 mutation carriers. Presented at the 43rd Annual Meeting of the ASCO, Chicago, IL, June 1–5, 2007; Abstr. No. 3529.
- (36) Banasik, M.; Komura, H.; Shimoyama, M.; Ueda, K. Specific inhibitors of poly(ADP-ribose) synthetase and mono(ADP-ribosyl)transferase. *J. Biol. Chem.* **1992**, *267*, 1569–1575.
- (37) Banasik, M.; Ueda, K. Inhibitors and activators of ADP-ribosylation reactions. *Mol. Cell. Biochem.* **1994**, *138*, 185–197.
- (38) Kamanaka, Y.; Kondo, K.; Ikeda, Y.; Kamoshima, W.; Kitajima, T.; Suzuki, Y.; Nakamura, Y.; Umemura, K. Neuroprotective effects of ONO-1924H, an inhibitor of poly ADP-ribose polymerase (PARP), on cytotoxicity of PC12 cells and ischemic cerebral damage. *Life Sci.* **2004**, *76*, 151–162.
- (39) Loh, V. M., Jr.; Cockcroft, X. L.; Dillon, K. J.; Dixon, L.; Drzewiecki, J.; Eversley, P. J.; Gomez, S.; Hoare, J.; Kerrigan, F.; Matthews, I. T.; Menear, K. A.; Martin, N. M.; Newton, R. F.; Paul, J.; Smith, G. C.; Vile, J.; Whittle, A. J. Phthalazinones. Part 1: the design and synthesis of a novel series of potent inhibitors of poly(ADP-ribose)polymerase. *Bioorg. Med. Chem. Lett.* **2005**, *15*, 2235–2238.
- (40) Cockcroft, X. L.; Dillon, K. J.; Dixon, L.; Drzewiecki, J.; Kerrigan, F.; Loh, V. M., Jr.; Martin, N. M.; Menear, K. A.; Smith, G. C. Phthalazinones 2: optimisation and synthesis of novel potent inhibitors of poly(ADP-ribose)polymerase. *Bioorg. Med. Chem. Lett.* **2006**, *16*, 1040–1044.
- (41) Lipinski, C. A.; Lombardo, F.; Dominy, B. W.; Feeny, P. J. Experimental and computational approaches to estimate solubility and permeability in drug discovery and development settings. *Adv. Drug Delivery Rev.* **1997**, *23*, 3–25.
- (42) Purnell, M. R.; Whish, W. J. Novel inhibitors of poly(ADP-ribose) synthetase. *Biochem. J.* **1980**, *185*, 775–777.
- (43) Dillon, K. J.; Smith, G. C.; Martin, N. M. A FlashPlate assay for the identification of PARP-1 inhibitors. *J. Biomol. Screening* **2003**, *8*, 347–352.
- (44) Skehan, P.; Storeng, R.; Scudiero, D.; Monks, A.; McMahon, J.; Vistica, D.; Warren, J. T.; Bokesch, H.; Kenney, S.; Boyd, M. R. New colorimetric cytotoxicity assay for anticancer-drug screening. *J. Natl. Cancer Inst.* **1990**, *82*, 1107–1112.
- (45) Hickson, I.; Zhao, Y.; Richardson, C. J.; Green, S. J.; Martin, N. M. B.; Orr, A. I.; Reaper, P. M.; Jackson, S. P.; Curtin, N. J.; Smith, G. C. M. Identification and characterization of a novel and specific inhibitor of the ataxia-telangiectasia mutated kinase ATM. *Cancer Res.* **2004**, *64*, 9152–9159.

JM8001263